Effects of Longitudinal Shifts of Centre of Gravity on Ship Resistance: A Case Study of a 31 M Hard-Chine Crew Boat

Ketut Suastika[1*], Soegeng Riyadi[1], I Ketut Aria Pria Utama[1], and Xuefeng Zhang[2]
[1]*Department of Naval Architecture, Institut Teknologi Sepuluh Nopember (ITS), Surabaya 60111, Indonesia*
[2]*School of Marine Science and Technology, Tianjin University, Tianjin, China*

Keywords: CFD, Longitudinal Shift of Centre of Gravity, Hard-chine Crew Boat, Ship Resistance, Wave Pattern.

Abstract: Computational fluid dynamics (CFD) simulations were performed to study effects of the longitudinal shifts of centre of gravity (from the designed one) on ship resistance. Such a shift of centre of gravity has been frequently observed in practice. This can occur, for example, due to inaccuracies in size and weight estimations of ship components in the design stage and imperfections in bending, welding and assembly processes in the production stage. For the reference case where there is no centre-of-gravity shift, the CFD results were verified using data obtained from towing-tank experiments and using results from the Savitsky's model. Results of analysis show that for relatively low Froude numbers, a forward shift of centre of gravity results in a decrease of ship resistance while a backward shift results in an increase of ship resistance. The opposite is true for relatively high Froude numbers. Because the boat is designed to operate in relatively high Froude numbers (Fr ¿ 0.7), a backward shift of centre of gravity is more favourable.

1 INTRODUCTION

In ship design, one of the owner requirements is the ship speed. Based on the owner requirements, a ship designer decides on the hull form and ship principal particulars. So, ship speed enters the ship design process in the first stage (EVANS, 1959). Estimations of ship resistance and the required powering then follow.

In the first instance, the ship resistance is estimated based on the full-load condition. However, a ship is not always in full-load condition during its operations. A shift of centre of gravity, particularly in the longitudinal direction, may take place if the loading condition changes. It has been observed that this longitudinal shift of centre of gravity affects the ship resistance (Kazemi and Salari, 2017).

A shift of centre of gravity, relative to the designed one, can also take place during the production process of the ship. This can happen due to, for example, oversize of main engine, inaccuracy in weight estimations of generator, structural components etc. In addition, a shift of centre of gravity can also occur due to imperfections in bending, welding and assembly processes (Takechi et al., 1998).

Figure 1 illustrates the production process of a hard-chine crew boat in PT. Orela Shipyard, Ujung Pangkah, Gresik, Indonesia and Figure 2 shows the construction part near the bow. The boat in production as shown in Figure 1 and 2 was made of aluminium. In such a production process, imperfections as described above can occur, which result in a (longitudinal) shift of centre of gravity relative to the designed one. Although longitudinal shifts of centre of gravity have frequently been observed in practice, its effects on ship resistance have insufficiently been explored.

The purpose of the present study is to investigate effects of the longitudinal shifts of centre of gravity on ship resistance. For that purpose, a hard-chine crew boat, designed and built by PT. Orela Shipyard, as shown in Figure 1 and 2, is considered as a case study. The ship principal-particulars are summarized in Table 1.

Computational fluid dynamics (CFD) simulations were performed and the results for the reference case without shift of centre of gravity were verified using data obtained from towing-tank experiments and using results from the Savitsky's model (Savitsky, 1964).

The research method is further elaborated in Section. 2. The results and discussion are presented in Section 3. The paper ends with conclusions, presented in Section 4.

Suastika, K., Riyadi, S., Utama, I. and Zhang, X.
Effects of Longitudinal Shifts of Centre of Gravity on Ship Resistance: A Case Study of a 31 m Hard-chine Crew Boat.
DOI: 10.5220/0008550801450152
In *Proceedings of the 3rd International Conference on Marine Technology (SENTA 2018)*, pages 145-152
ISBN: 978-989-758-436-7

Figure 1: A Hard-chine Crew Boat during The Production Process (courtesy of PT. Orela Shipyard).

Figure 2: Construction Part of The Hard-chine Orela Crew Boat Near The bow (courtesy of PT. Orela Shipyard).

2 METHOD

Computational fluid dynamics (CFD) (Anderson, 1994; Versteeg et al., 1995; Moukalled et al., 2016) are utilized to simulate effects of the longitudinal shift of centre of gravity (relative to the designed one) on ship resistance. Table 2 summarizes variations of position of the centre of gravity in the longitudinal direction considered in the present study. As mentioned above, for the reference case where there is no shift of centre of gravity (Case 0), the CFD results are verified using data obtained from towing-tank experiments and using results from the Savitsky's model (Savitsky, 1964).

Table 1: Ship Principal-particulars of The Crew Boat.

Length Overall (LOA)	31.20 m
Length Between Perpendicular (L_{PP})	28.80 m
Breadth (B)	6.80 m
Depth (H)	2.75 m
Draft (T)	1.40 m
Maximum Speed (V_{max})	26 kn
Displacement (Δ)	104.68 t

2.1 Towing-tank Experiments

Towing-tank experiments were performed at the Hydrodynamics Laboratory, Faculty of Marine Technology, Institut Teknologi Sepuluh Nopember (ITS), Surabaya, Indonesia. The dimension of the tank is as follows: length = 50.0 m, width = 3.0 m, maximum water depth = 2.0 m and maximum towing speed = 4.0 m/s.

A model of the ship was built from fibreglass reinforced plastic (FRP) coated with paint and resin. The geometrical scale between model and prototype is 1:40. The Froude scaling was applied between the full scale and model ship in the experiments. The ship resistance was measured using a load cell. Before performing a test, the load cell was calibrated by using a mass of 0.5 kg.

The ship speeds tested were 11, 14, 17, 20, 23 and 26 knots (full-scale speed). These correspond to model speeds of 0.894, 1.14, 1.38, 1.63, 1.87 and 2.11 m/s, respectively. The Froude-number range is approximately between 0.4 to 0.8. At Fr ¡ 0.5 the ship is expected to reveal displacement characteristics while at Fr ¿ 0.7 it is expected to reveal semi-displacement characteristics. Figure 3 shows the ship model towed at 20 kn (Fr = 0.62).

2.2 CFD Simulations

CFD simulations were performed to calculate the ship resistance for varying ship speed and varying position of centre of gravity. The speed variations are in accordance to the speeds measured in the towing-tank experiments. The variations of centre-of-gravity position are as summarized in Table 2.

The CFD simulations utilized the software package Numeca Fine/Marine®(Marine Fine, 2013), which is based on a finite volume method (FVM). The ISIS-CFD code of the package solves the incompressible unsteady Reynolds-averaged Navier-Stokes (RANS) equations for modelling turbulent multi-

Table 2: Variations of Longitudinal Position of Centre of Gravity Considered in The Study (measured from the aft perpendicular).

Case 0	1.00 LCG (design) 12.45 m (+0.0m)
Case 1	1.03 LCG 12.85 m (+0.4m)
Case 2	1.02 LCG 12.65 m (+0.4m)
Case 3	0.98 LCG 12.25 m (-0.2m)
Case 4	0.97 LCG 12.05 m (-0.4m)

Figure 3: Ship Model of The 31 m Hard-chine Crew Boat Towed at 20 knots (Fr =0.62).

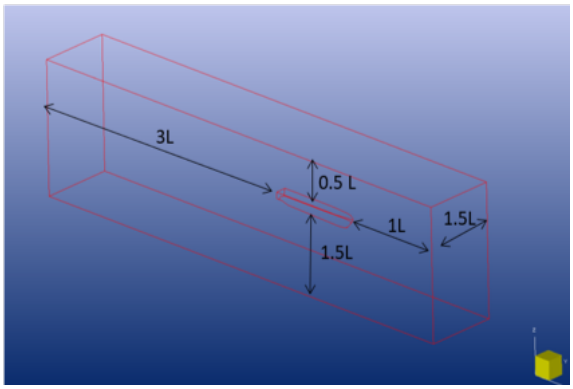

Figure 4: A Sketch of The Computational Domain

phase flows with appropriate boundary conditions. It utilizes the volume of fluid (VOF) method to resolve the free surface boundary (Hirt and Nichols, 1981), that is, modelling of the generation of waves. The mass, momentum and volume-fraction conservation equations are represented, respectively, as follows:

$$\frac{\partial}{\partial t}\int_v \rho dV + \int_S \rho(U-U_d)\cdot ndS = 0 \tag{1}$$

$$\frac{\partial}{\partial t}\int_v \rho U_i dV + \int_S \rho U_i(U-U_d)\cdot ndS = \int_s(\tau_{ij}I_j - pI_i)\cdot ndS + \int_V \rho g_i dV \tag{2}$$

$$\frac{\partial}{\partial t}\int_v c_i dV + \int_S c_i(U-U_d)\cdot ndS \tag{3}$$

In Equation (1), (2) and (3), V is the control volume, bounded by the closed surface S with a normal vector n directed outward moving at the velocity U_d, U is the velocity field and p is the pressure field. Furthermore, τ_{ij} is the turbulent (Reynolds) stress tensor, g_i is the component of the gravity vector, I_j is a vector whose components are zero except for j=1 and c_i is the volume fraction of fluid i and is used to distinguish the presence (c_i = 1) and the absence (c_i = 0) of fluid i.

The turbulence model used is the SST k-ω model (SST for shear-stress transport), where k is the turbulent kinetic energy and ω is the specific dissipation rate (Menter, 1994)(ISIS-CFD, 2013). The main feature of the model is zonal blending of modelling, using the Wilcox's k-ω model for the flow near solid walls and using the standard k-εmodel (transformed into k-ω formulation) for the flow near boundary layer edges and in free-shear layers. The transport equations for k and ω are represented as follows, where the blending coefficient F_1 models the coefficients of the original ω and eε.

$$\frac{\partial \rho k}{\partial t} + \frac{\partial}{\partial x_j}\left(\rho U_j k - (\mu + \sigma_\omega \mu_t)\frac{\partial k}{\partial x_j}\right) = \tau_{t_{ij}} S_{ij} - \beta\rho\omega k \tag{4}$$

$$\frac{\partial \rho \omega}{\partial t} + \frac{\partial}{\partial x_j}\left(\rho U_j \omega - (\mu + \sigma_\omega \mu_t)\frac{\partial \omega}{\partial x_j}\right) = P_\omega - \beta\rho\omega^2 + 2(1-F_1)\frac{\rho\sigma_{\omega^2}}{\omega}\frac{\partial k}{\partial x_j}\frac{\partial \omega}{\partial x_j} \tag{5}$$

Details of the model are described in (11). The cell size near the wall, y_{wall}, is calculated based on the wall variable y^+, which is given as follows:

$$y^+ = \frac{\rho u_t y_{wall}}{\mu} \tag{6}$$

where $u_\tau = \sqrt{\frac{\tau_{wall}}{\rho}} = \sqrt{\frac{1}{2}\rho(V_{reff}^2)C_f}$ is the friction velocity. The value of y_{wall} is calculated as

$$y_{wall} = 6\frac{\nu_{ref}}{\nu}^{7/8}\frac{L_{ref}}{2}^{1/8} y^+ \tag{7}$$

In the simulations, the value for y^+ is set equal to 10 and the length between the perpendiculars (L_{PP}) is used as the reference length L_{ref}.

The computational domain is sketched in Fig 4. Due to symmetry, only a half of the ship is modelled. The inlet is located at 1.0L upstream from the vessel, while the outlet is located at 3.0L downstream from the vessel. The side wall is 1.50L aside the vessel. The bottom wall is located at 1.50L below the vessel and the top wall is located at 0.50L above the vessel (L is the length between the perpendiculars L_{PP}). The boundary conditions (according to the definitions used in Numeca Fine/Marine®) are summarized in Table 3.

It is well-known that, in the application of a numerical method, there is a trade-off between accu-

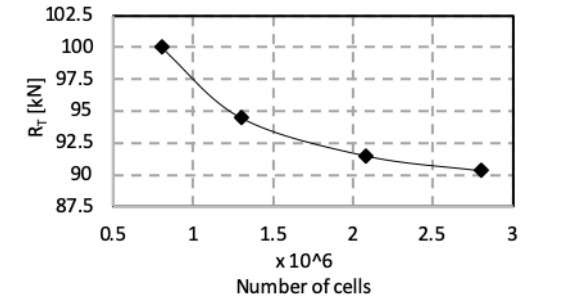

Figure 5: Total Ship Resistance as Function of Number of Cells for Ship Speed of 20 knots (Fr = 0.62).

racy (which depends on the number of computational cells) and computational cost. To find an optimum number of cells used in the simulations, grid-independence tests were performed as illustrated in Figure 5. As shown in Figure. 5, the total ship resistance decreases monotonically with increasing number of cells (elements). The total resistance is expected to reach an asymptotic value for very large number of cells (theoretically, if the number of cells tends to infinity). Due to the limited capacity of available hardware, the number of cells of 2.8 x 106 was considered as the most optimum number of cells in the present study.

Results of the meshing are shown in Figure. 6 and 7, respectively, for (a half of) the ship hull and the computational domain with the ship model therein. The total number of cells in the latter case is 2.8 x 106. This number of cells has also been utilized in a previous study utilizing the same crew boat where effects of the application of a Hull Vane®on ship resistance was studied (Riyadi and Suastika, 2018).

Table 3: Boundary Conditions

Description	Type	Condition
Inlet (Xmin)	EXT	Far field, Vx = 0
Outlet (Xmax)	EXT	Far field, Vx = 0
Bottom (Zmin)	EXT	Update hydrostatic pressure
Top (Zmax)	EXT	Update hydrostatic pressure
Side (Ymin)	MIR	Mirror
Side (Ymax)	EXT	Far field, Vx = 0
Ship hull	SOL	Wall function
Ship deck	SOL	Free slip (zero shear stress)
Motion	Translation in X direction with a given speed	Speed = Ship speed, using one half sinusoidal ramp
	Translation in Z direction with solved motion type	Linear law
	Rotation in Ry (pitch) with solved motion type	Linear law
Convergence criteria	Order of magnitude of residual decrease	Second order

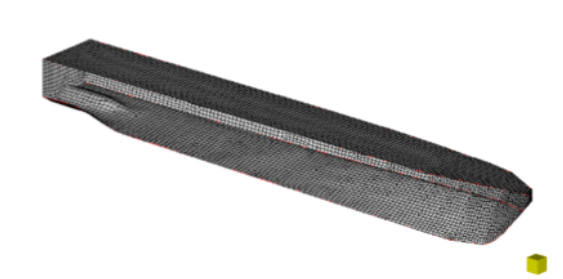

Figure 6: Mesh of A Half of The Ship Hull.

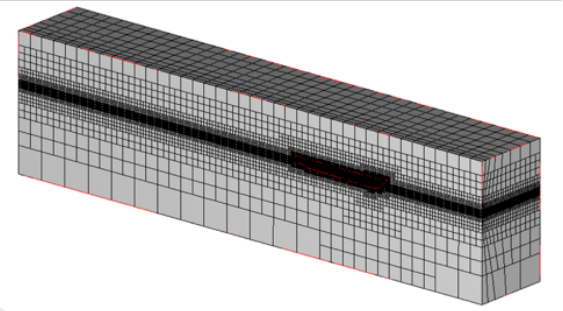

Figure 7: Computational Domain with The Ship Model Therein. The total number of cells is 2.8 x 10^6.

3 RESULTS AND DISCUSSIONS

To verify the CFD results, these are compared with those obtained from Savitsky's model and experimental data (towing-tank experiments). Figure 8 shows a comparison of total ship resistance as function of Froude number obtained from CFD, Savitsky's model (Savitsky, 1964) and towing-tank experiments for the reference case (Case 0; see Table 2). For relatively low Froude numbers (Fr ¡ 0.45) and for relatively high Froude numbers (Fr ¿ 0.7), the CFD and Savitsky's results underestimate the experimental data. The average relative error between the results of CFD and Savitsky's model (Savitsky, 1964) is 2.5% and that between CFD results and towing-tank data is 2.9%, which are relatively small.

A hump region is observed in the Froude number range between approximately 0.45 and 0.70. In this hump region the results from CFD and Savitsky's model (Savitsky, 1964) overestimate the experimental data. Furthermore, the CFD and Savitsky's results show the hump region more clearly than the towing-tank results. However, generally, the three curves show a similar trend. Such a hump region

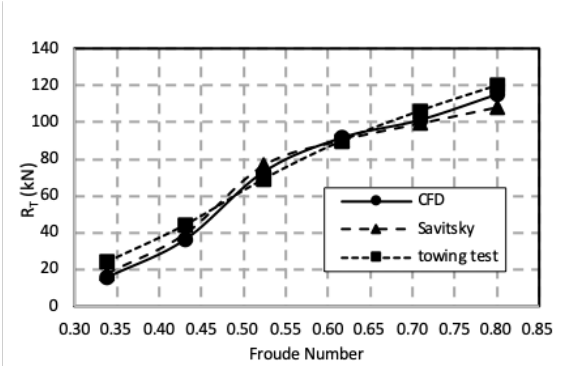

Figure 8: Total Ship Resistance as Function of Froude Number, obtained from CFD, Savitsky (Savitsky, 1964) and Towing-tank Experiments.

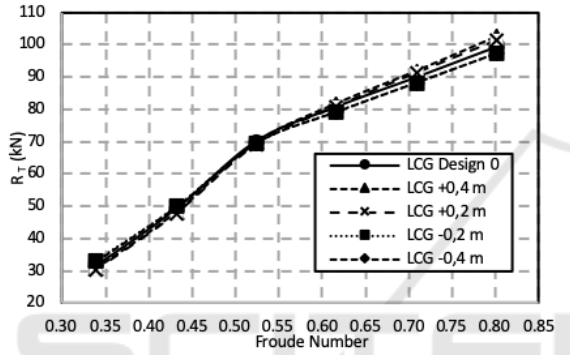

Figure 9: Total Ship Resistance as Function of Froude Number for the Five Cases as summarized in Table 2.

has been observed in earlier studies (Yousefi et al., 2013)(Suastika et al., 2017) For Fr ¡ 0.45, the hydrostatic forces (weight and buoyancy) are dominant. On the other hand, for Fr ¿ 0.7 the hydrodynamic force becomes more dominant than the hydrostatic forces.

Effects of the longitudinal shifts of centre of gravity on ship resistance are investigated using CFD simulations. In the simulations, the ship displacement is kept constant.

Figure 9 shows the total ship resistance as function of Froude number for the five cases as summarized in Table 2. The difference in ship resistance from the five curves as shown in Figure 9 is rather small and difficult to be distinguished. To make the difference clearer, Figure 10 shows the percentage of relative difference compared to the reference case (Case 0). As shown in Figure 10, for relatively low Froude numbers (say Fr ¡ 4.5), a forward shift of centre of gravity results in a decrease of ship resistance but a backward shift results in an increase of ship resistance. On the contrary, for relatively high Froude numbers (say Fr ¿ 0.6), a forward shift of centre of gravity results in an increase of ship resistance but a backward shift results in a decrease of ship resistance.

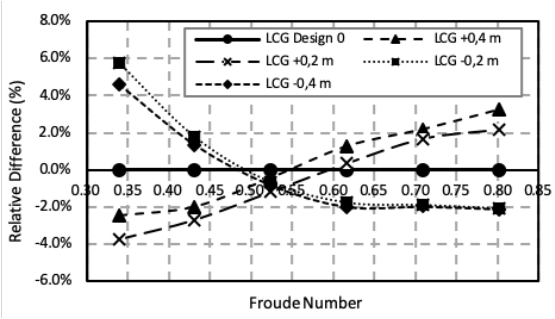

Figure 10: Relative Difference in Ship Resistance Compared to The Reference Case (Case 0; LCG design).

Due to the shift of centre of gravity, the ship resistance can increase approximately 6% in the lowest Froude number (Case 3; LCG - 0.2 m) and approximately 3% in the highest Froude number (Case 1; LCG + 0.4 m). Furthermore, the decrease can reach approximately 4% in the lowest Froude number (Case 2; LCG + 0.2 m) and approximately 2% in the highest Froude number (Case 3; LCG - 0.2 m and Case 4; LCG - 0.4 m). Which shift is more favourable, it depends on the operational scheme of the boat. If, in most of the time, it is operated at relatively large speed (say Fr ¿ 0.6) then the backward shift of centre of gravity is more favourable.

Figure 11 shows wave patterns for the different cases as summarized in Table 2 with Fr = 0.34. Figure 12 shows locations of measurement points of free-surface elevation (water level) near the ship hull. In addition, Figure 13 shows wave patterns for the different cases with Fr = 0.80. The wave pattern for Fr = 0.34 is very different from that for Fr = 0.80 (compare for example Figure 11a with Figure 13a), as may be expected, because of the very different Froude numbers. For Fr = 0.34, two wave crests and two wave troughs are observed along the ship while for Fr = 0.80 only one wave crest and one wave trough are observed.

For Fr = 0.34, a forward shift of centre of gravity (Case 1 and 2) results in a deeper wave trough in front of the midship (points 3 and 4 in Figure 12) while a backward shift results in a higher wave through in front of the midship, compared to the reference case (see also Table 4). Near the bow (points 1 and 2), a forward shift results in an increase of water level but a backward shift results in a decrease of the water level. Furthermore, near the stern (points 9, 10 and 11), a forward shift results also in an increase of water level but a backward shift results in a decrease of the water level.

For Fr = 0.80, a forward shift of centre of gravity results in a higher wave trough in front of the mid-

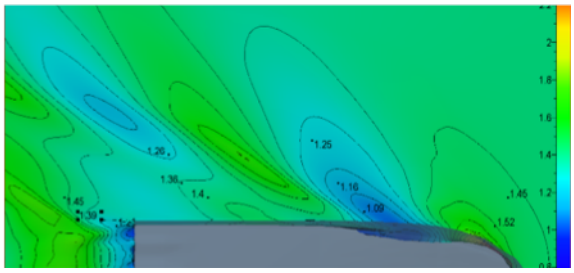

(a) Case 0; $Fr = 0.34$

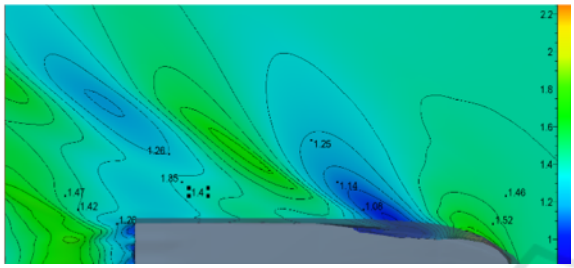

(b) Case 0(+0.4m); $Fr = 0.34$

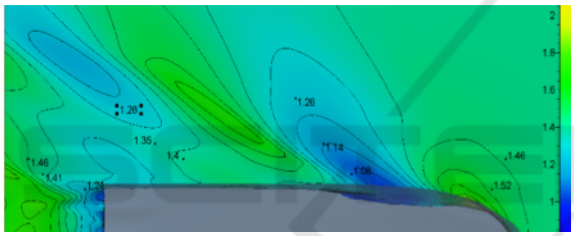

(c) Case 0(+0.2m); $Fr = 0.34$

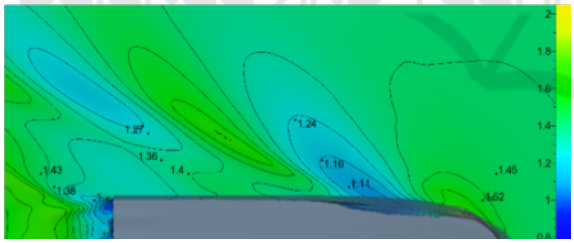

(d) Case 0(-0.2m); $Fr = 0.34$

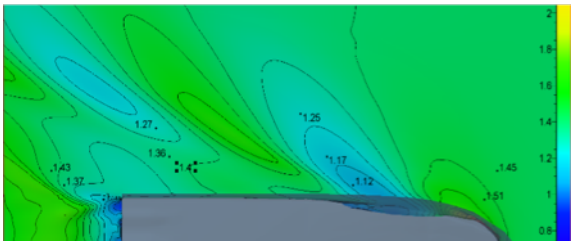

(e) Case 0(-0.4m); $Fr = 0.34$

Figure 11: Contour of Water Surface Elevation (water level η) for Different Cases as summarized in Table 2 with $Fr = 0.34$. The reference plane is at the base line (keel), which is 1.40 m below the mean water surface.

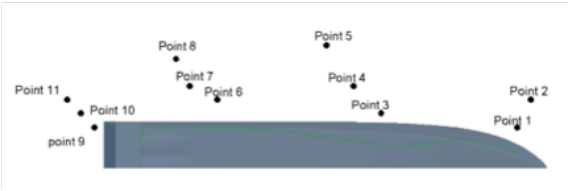

Figure 12: Locations of Measurement Points of Free Surface Elevation (water level) near the Ship Hull.

Table 4: Water Level η at The Measurement Points as shown in Figure 12, Relative to The Water Level for The Reference Case (Case 0) η_0 The Reference Horizontal Plane is at The Base Line, which is 1.40 m below The Mean Water Surface. The Froude Number $Fr = 0.34$.

Point	Case 0 η_0 [m]	Case 1 $\eta - \eta_0$ [m]	Case 2 $\eta - \eta_0$ [m]	Case 3 $\eta - \eta_0$ [m]	Case 4 $\eta - \eta_0$ [m]
1	1.52	0.00	0.00	0.00	-0.01
2	1.45	+0.01	+0.01	0.00	0.00
3	1.09	-0.01	-0.01	+0.01	+0.03
4	1.16	-0.02	-0.02	0.00	+0.01
5	1.25	0.00	+0.01	-0.01	0.00
6	1.40	0.00	0.00	0.00	0.00
7	1.35	0.00	+0.01	-0.01	0.00
8	1.26	0.00	0.00	+0.01	+0.01
9	1.21	+0.05	+0.03	-0.01	-0.03
10	1.39	+0.03	+0.02	-0.01	-0.02
11	1.45	+0.02	+0.01	-0.02	-0.02

ship (points 3 and 4 in Figure 12) while a backward shift results in a lower wave through compared to the reference case (see Table 5). This is also the case for the region near the bow (points 1 and 2), that is, an increase of water level due to a forward shift but a decrease of water level due to a backward shift. Behind the midship (points 5, 6 and 7), a forward shift results in a decrease of water level while a backward shift

Table 5: Water Level η at The Measurement Points as shown in Figure 12, Relative to The Water Level for The Reference Case (Case 0) η_0 The Reference Horizontal Plane is at The Base Line, which is 1.40 m below The Mean Water Surface. The Froude Number $Fr = 0.34$.

Point	Case 0 η_0 [m]	Case 1 $\eta - \eta_0$ [m]	Case 2 $\eta - \eta_0$ [m]	Case 3 $\eta - \eta_0$ [m]	Case 4 $\eta - \eta_0$ [m]
1	1.45	+0.01	0.00	0.00	-0.01
2	1.43	0.00	0.00	0.00	-0.01
3	1.78	+0.03	+0.01	-0.01	-0.03
4	1.59	+0.03	+0.02	-0.01	-0.01
5	1.52	-0.01	-0.01	+0.01	0.00
6	1.37	-0.05	-0.03	+0.03	+0.05
7	1.42	-0.03	-0.02	+0.02	+0.06
8	1.56	0.00	0.00	-0.01	0.00
9	0.76	+0.03	+0.01	-0.01	-0.02
10	0.86	0.00	-0.01	+0.01	+0.03
11	0.79	0.00	0.00	0.00	+0.01

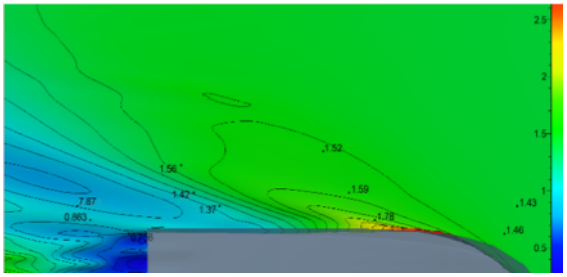

(a) Case 0; $Fr = 0.8$

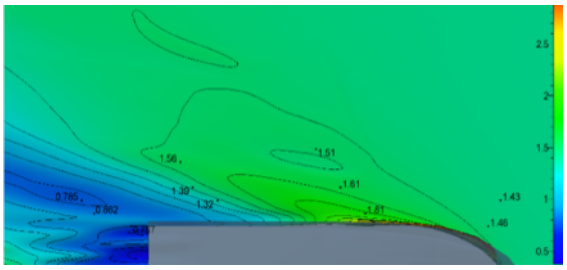

(b) Case 0(+0.4m); $Fr = 0.8$

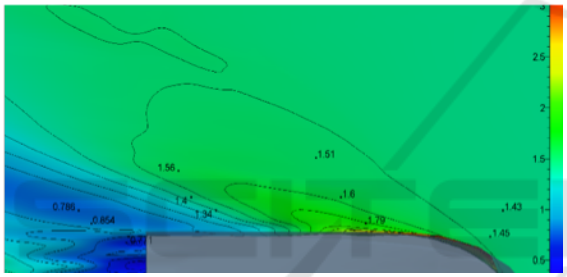

(c) Case 0(+0.2m); $Fr = 0.8$

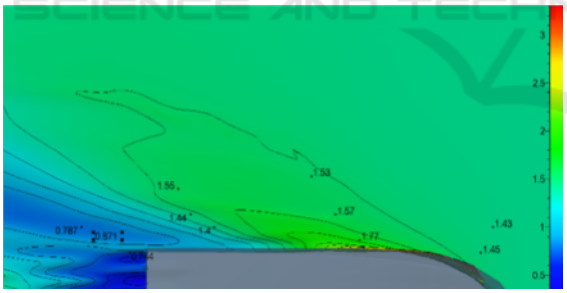

(d) Case 0(-0.2m); $Fr = 0.8$

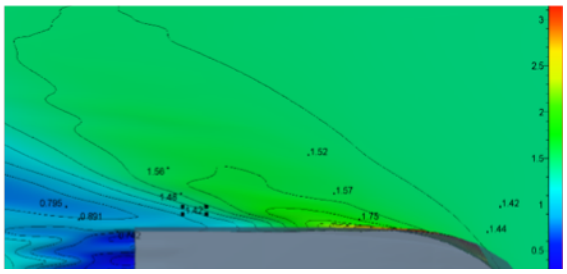

(e) Case 0(-0.4m); $Fr = 0.8$

Figure 13: Contour of Water Surface Elevation (water level η) for Different Cases as summarized in Table 2 with $Fr = 0.8$. The reference plane is at the base line (keel), which is 1.40 m below the mean water surface.

results in an increase of water level.

A forward shift of centre of gravity results in a different wave pattern compared to a backward shift. This difference of wave pattern results in different wave resistance, which ultimately affects the total resistance as discussed above. The above observations characterize the hull form of the hard-chine crew boat.

4 CONCLUSIONS

CFD simulations were performed to study effects of the longitudinal shifts of centre of gravity on ship resistance. For the reference case where there is no centre-of-gravity shift, the CFD results are verified using data from towing-tank experiments and results from the Savitsky's model (Savitsky, 1964). Centre-of-gravity shifts can occur in practice due to, for example, oversize of main engine, inaccuracy in weight estimations of generator, structural components etc. It can also occur due to imperfections in bending, welding and assembly processes.

For relatively low Froude numbers (say Fr ¡ 4.5), where the hydrostatic forces are dominant, a forward shift of centre of gravity results in a decrease of ship resistance but a backward shift results in an increase of ship resistance. On the contrary, for relatively high Froude numbers (say Fr ¿ 0.6), where the hydrodynamic forces are dominant, a forward shift of centre of gravity results in an increase of ship resistance but a backward shift results in a decrease of ship resistance.

It depends on the operational scheme of the ship which longitudinal shift of centre of gravity is more favourable. In the present case, where the boat is designed to operate in a semi-planing mode (Fr ¿ 0.7), a backward shift of centre of gravity is more favourable.

The wave pattern for relatively low Froude numbers (Fr ¡ 0.45) is very different from that for relatively high Froude numbers (Fr ¿ 0.7). For relatively low Froude numbers, two wave crests and two wave troughs were observed along the ship while for relatively high Froude numbers only one wave crest and one wave trough were observed.

A forward shift of centre of gravity results in a different wave p]attern compared to a backward shift. This difference of wave pattern results in different wave resistance, which ultimately affects the total ship resistance. The resulting wave pattern is characteristic for the hull form being investigated.

ACKNOWLEDGEMENTS

Ketut Suastika was a visiting researcher at the School of Marine Science and Technology, Tianjin University, China, in the period from October 10th, 2018 to January 9th, 2019 where parts of the present study were carried out. He thanks the School of Marine Science and Technology, Tianjin University, China, for the opportunity having been provided. This research project was supported by the Ministry of Research, Technology and Higher Education (Ristekdikti) of the Republic of Indonesia, under the grant Penelitian Terapan Unggulan Perguruan Tinggi (PTUPT) with contract no. 1031/PKS/ITS/2018.

REFERENCES

Anderson, J. D. (1994). *Computational fluid dynamics : the basics with applications*. McGraw-Hill, New York.

EVANS, J. H. (1959). BASIC DESIGN CONCEPTS. *Journal of the American Society for Naval Engineers*, 71(4):671–678.

Hirt, C. W. and Nichols, B. D. (1981). Volume of fluid (VOF) method for the dynamics of free boundaries. *Journal of Computational Physics Journal of Computational Physics*, 39(1):201–225.

ISIS-CFD (2013). *Theoretical Manual*. EMN, Ecole Centrale de Nantes.

Kazemi, H. and Salari, M. (2017). Effects of Loading Conditions on Hydrodynamics of a Hard-Chine Planing Vessel Using CFD and a Dynamic Model. *International Journal of Maritime Technology*, 7(0):11–18.

Marine Fine (2013). *User Manual Flow Integrated Environment for Marine Hydrodynamic*. Numeca International, Belgium.

Menter, F. R. (1994). Two-Equation Eddy-Viscosity Turbulence Models for Engineering Applications. *AIAA journal.*, 32(8):1598.

Moukalled, F., Mangani, L., and Darwish, M. (2016). *The Finite Volume Method in Computational Fluid Dynamics : an Advanced Introduction with OpenFOAM and Matlab*. Springer.

Riyadi, S. and Suastika, K. (2018). Experimental and numerical study of high Froude-number resistance of ship utilizing a Hull Vane®: A case study of a hard-chine crew boat. In *Proc.11th International conference on marine technology*. MARTEC.

Savitsky, D. (1964). Hydrodynamic Design of Planing Hulls. *Marine Technology and SNAME News*, 1(04):71–95.

Suastika, K., Hidayat, A., and Riyadi, S. (2017). Effects of the application of a stern foil on ship resistance: A case study of an orela crew boat. *International Journal of Technology*, 8:1266.

Takechi, S., Aoyama, K., and Nomoto, T. (1998). Basic studies on accuracy management system based on estimating of weld deformations. *Journal of the Society of Naval Architects of Japan*, 3:194–200.

Versteeg, H., Malalasekera, W., Orsi, G., Ferziger, J. H., Date, A. W., and Anderson, J. D. (1995). *An Introduction to Computational Fluid Dynamics - The Finite Volume Method*.

Yousefi, R., Shafaghat, R., and Shakeri, M. (2013). Hydrodynamic analysis techniques for high-speed planing hulls. *Applied Ocean Research*, 42:105–113.